Available online at www.sciencedirect.com
SCIENCE DIRECT
Thermochimica Acta 444 (2006) 6–12
thermochimica acta
www.elsevier.com/locate/tca

# Thermokinetic study of the oxidation of $ZrAl_3$ powders

H. Geßwein*, J.R. Binder

*Forschungszentrum Karlsruhe, Institut für Materialforschung III, Postfach 3640, 76021 Karlsruhe, Germany*

Received 1 September 2005; received in revised form 30 January 2006; accepted 7 February 2006
Available online 23 March 2006

**Abstract**

The oxidation kinetics of ball milled $ZrAl_3$ powder was investigated by thermogravimetry at temperatures up to 1100 °C. The non-selective oxidation of $ZrAl_3$ results in the formation of $\alpha$-$Al_2O_3$, tetragonal and monoclinic $ZrO_2$. Non-isothermal and isothermal measurements were simultaneously used in a multivariate non-linear regression analysis to determine the kinetic reaction parameters. The oxidation process is well described by a generalized *n*-dimensional Avrami type rate equation, according to a diffusion limited growth reaction with an apparent activation energy of 244 kJ/mol. Significant improvement of the fit quality of the kinetic data is achieved through a two-step kinetic model indicating a complex oxidation mechanism.


*Keywords:* Kinetics; Oxidation; $ZrAl_3$; Thermogravimetry

## 1. Introduction

Reaction bonding processes such as RBAO (reaction bonded aluminum oxide) [1] and RBSN (reaction bonded silicon nitride) [2] offer a number of advantages compared to conventional ceramic fabrication routes. One of the most important is the near-net shape capability which makes these techniques suitable for the manufacture of complex shapes produced by either slip casting, injection moulding or machining of green bodies [3]. The low sinter shrinkage and the resulting high dimensional accuracy of reaction formed ceramics is achieved through volume expansion during gas–solid reactions.

The use of intermetallic compounds such as $ZrSi_2$ offers the advantage of a much higher volume increase during oxidation compared to pure metals like aluminum or silicon [4]. Another promising reactive precursor material for the fabrication of shrinkage-free dense oxide ceramics is the intermetallic compound $ZrAl_3$ [5]. Reaction bonded alumina-zirconia composites can be produced by the reaction of $ZrAl_3$ green body with an oxygen-containing atmosphere according to the following reaction scheme:

$$ZrAl_{3(s)} + 13/4O_{2(g)} \longrightarrow ZrO_{2(s)} + 3/2Al_2O_{3(s)}$$

During this exothermic reaction a large amount of heat is set free and local overheating of the green body may occur. This can lead to sharp thermal and concentration gradients that cause stresses which result in sample cracking. Therefore reaction control, i.e. a careful temperature control during the oxidation reaction, is essential for the production of high-quality reaction bonded ceramics. Knowledge of the oxidation kinetics can be used to avoid uncontrolled reactions.

There are only a few studies on the oxidation of intermetallic phases in the system Zr–Al and these mainly focus on the oxidation of bulk materials [6–8]. This paper deals with the heterogeneous oxidation of $ZrAl_3$ particles in a gaseous oxidant. The oxidation kinetics of $ZrAl_3$ powder was studied by non-isothermal and isothermal thermogravimetry at temperatures up to 1100 °C. The aim of the kinetic analysis was to determine a kinetic model with minimal adjustable parameters which quantitatively describes the kinetic data. In the first step a model-free isoconversion method was used to obtain starting parameters for the non-linear regression model-fitting procedure which was carried out with the help of the Netzsch *Thermokinetics* software [9].

## 2. Materials and methods

The starting material used is $ZrAl_3$ (Alfa Aesar, 99%, metals basis) in the form of lumps. To reduce the particle size, the

* Corresponding author. Tel.: +49 7247 82 4055; fax: +49 7247 82 4612.
*E-mail address:* holger.gesswein@imf.fzk.de (H. Geßwein).

0040-6031/$ – see front matter © 2006 Elsevier B.V. All rights reserved.
doi:10.1016/j.tca.2006.02.010

material was cryo-milled for 0.25 h in liquid nitrogen (Spex CertiPrep Freezer/Mill 6800). After cryo-milling, the aluminide was passed through a 125 μm sieve and finally milled for 16 h in a planetary ball mill (Fritsch Pulverisette 5) with $ZrO_2$ milling balls in 2-propanol. One hundred grams of the aluminide and 100 g of 2-propanol were used during ball milling. The gas atmosphere in the 500 ml vial was surrounding air. To determine the amount of $ZrO_2$ impurities the $ZrO_2$ milling media was weighed before and after the milling step. The amount of $ZrO_2$ wear debris revealed by gravimetry was <0.2 wt.%.

The kinetic parameters were extracted from the experimental weight change data using following transformation:

$$\alpha = \frac{m_0 - m_t}{m_0 - m_\infty} \quad (1)$$

where $\alpha$ is the general variable reaction degree, $m_0$ the starting sample mass, $m_t$ the sample mass at time $t$ and $m_\infty$ is the sample mass after complete oxidation.

The oxidation kinetics of the ball milled powder was investigated by thermogravimetric analysis in a Netzsch STA 449C simultaneous thermal analyzer operated in TG mode. The oxidations were carried out under artificial air (20.5% $O_2$ in $N_2$) at a gas flow in the thermal analyzer of 50 ml/min. The TG baselines were corrected by subtraction of predetermined baselines run under identical conditions except for the absence of a sample. For kinetic analysis about 60 mg of $ZrAl_3$ were filled into the manufacturer's alumina crucible (15.7 mm diameter) that was then heated at 1, 2.5, 5 and 10 °C/min to 1100 °C. Additionally isothermal runs were performed at temperatures of 500, 600, 700 and 800 °C for several hours. A constant heating rate of 10 °C/min to the desired oxidation temperature was used in the isothermal runs.

The oxidation products were characterized by means of X-ray diffraction using a Siemens diffractometer (Model D5005) with Cu Kα radiation and a secondary graphite monochromator. The operating conditions were 40 kV and 40 mA in the angular range 20–80° in $2\theta$. Crystalline phase identification based on XRD patterns was aided by the ICDD-PDF database.

## 3. Results and discussion

### 3.1. Oxidation of $ZrAl_3$ powder

The surface area of the ball-milled powder, determined by BET analysis, was 1.5 $m^2$/g. Assuming spherical particles, a mean grain diameter of 1 μm was estimated using the relation $d_{BET} = 6/\rho S_{BET}$, where $\rho$ is the theoretical density of the aluminide ($\rho = 4.12$ g/$cm^3$) and $S_{BET}$ is the BET surface area. This average grain diameter is an effective particle size describing the reactivity of the powder. Fig. 1 shows the SEM micrograph of the ball-milled $ZrAl_3$ sample. The $ZrAl_3$ particles have an irregular morphology with sizes ranging between 1 and 5 μm, which is in reasonable agreement with the BET measurements.

The theoretical mass gain during complete $ZrAl_3$ oxidation is 60.4 wt.%. The maximum mass gain after complete oxidation of the 16 h ball milled powder is about 57 wt.% indicating a preoxidation of about 3.4 wt.% of the intermetallic compound

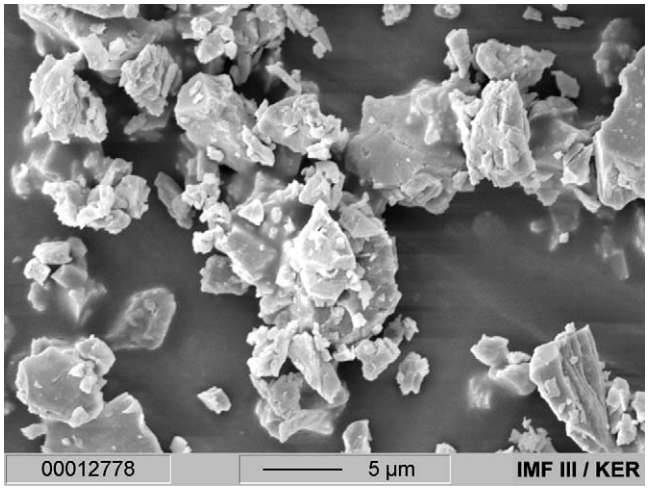


Fig. 1. SEM micrograph of ball milled (16 h in a planetary ball mill) $ZrAl_3$ powder.

during milling. The resulting passivating oxide film allows a safe handling of the powder. As can be seen from the XRD spectra in Fig. 2 the $ZrAl_3$ powder contains small amounts of a hexagonal $ZrAl_2$ phase. Impurity phases, like carbides and nitrides, which may have been formed during cryo-milling in liquid nitrogen and ball-milling in 2-propanol, were not detected.

Simultaneous DSC-TG-DTG curves for $ZrAl_3$ are presented in Fig. 3. It is evident that the shape of the DSC signal is consistent with that of the DTG except for the sharp exothermic peak at 960 °C. This indicates that the mass gain rate results from the corresponding reactions associated with the exothermic effect. The sample mass continously increases from 500 to 900 °C and is associated with the oxidation process of $ZrAl_3$. The exothermic peak at about 960 °C is related to the crystallisation of metastable transition alumina (formation of γ- or δ-$Al_2O_3$, see Fig. 4). This is discussed in the next paragraph.

Fig. 4 displays X-ray diffraction patterns of $ZrAl_3$ powders oxidized at 600 °C for 12 h and at 800, 900, 1000 and 1100 °C for 5 h. The sample exposed at temperatures of 600 °C shows diffraction peaks corresponding to unreacted $ZrAl_3$. The increased pattern background between 25° and 35° $2\theta$ clearly

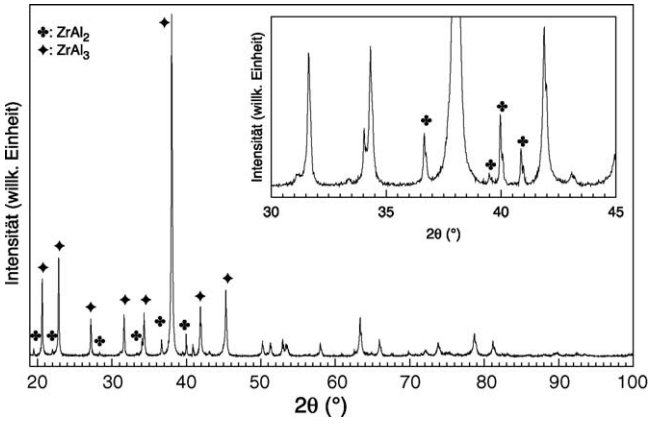


Fig. 2. XRD pattern of 16 h ball milled $ZrAl_3$ powder. The inset shows additional reflexes of small amounts of hexagonal $ZrAl_2$.

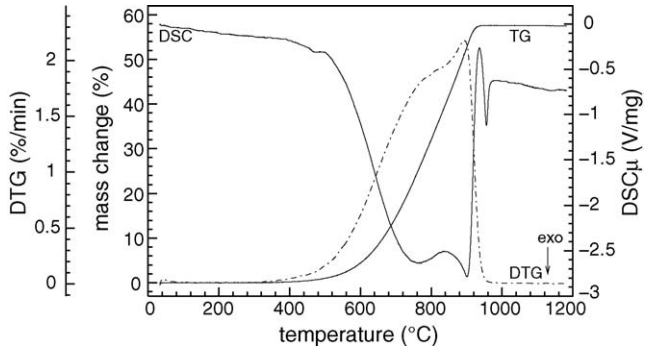


Fig. 3. DSC-TG-DTG curves recorded during heating of ball milled $ZrAl_3$ powder up to 1200 °C at a rate of 10 °C/min in flowing air (sample mass ∼15 mg).

indicates the formation of amorphous oxidation products. At 800 °C no more $ZrAl_3$ can be detected and the pattern consists of broad diffraction peaks of a tetragonal zirconia phase and of very weak diffuse peaks at 32–33 and 45–47° 2$\theta$ related to transition aluminas [10]. The exact crystallographic modification of the transition aluminas (γ-, δ- or θ-$Al_2O_3$) is not evident from this spectra because of weak diffraction intensities. At 900 and 1000 °C the intensities of these diffraction peaks slightly increase and at a temperature of 1100 °C the formation of α-$Al_2O_3$ can be observed. From this diffraction pattern the presence of θ-$Al_2O_3$ is clearly visible (see inset of Fig. 4(e)). The sample oxidized at 1100 °C for 5 h consists of tetragonal $ZrO_2$, θ-$Al_2O_3$, α-$Al_2O_3$ and a trace of monoclinic $ZrO_2$.

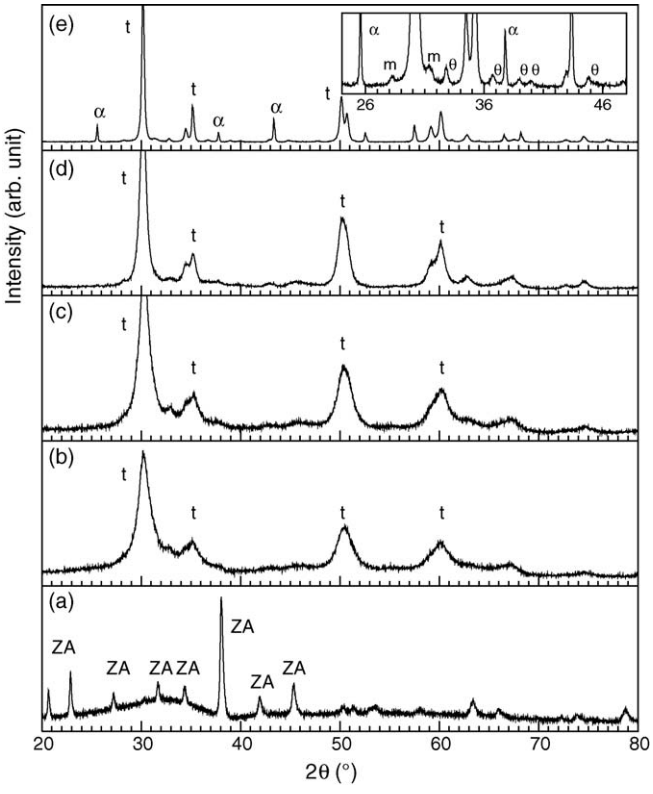


Fig. 4. XRD patterns of $ZrAl_3$ powder oxidized at (a) 600 °C for 12 h, (b) 800 °C, (c) 900 °C, (d) 1000 °C and (e) 1100 °C for 5 h under flowing air (ZA: $ZrAl_3$, t: t-$ZrO_2$, m: m-$ZrO_2$, $\alpha$: α-$Al_2O_3$ and θ: θ-$Al_2O_3$).

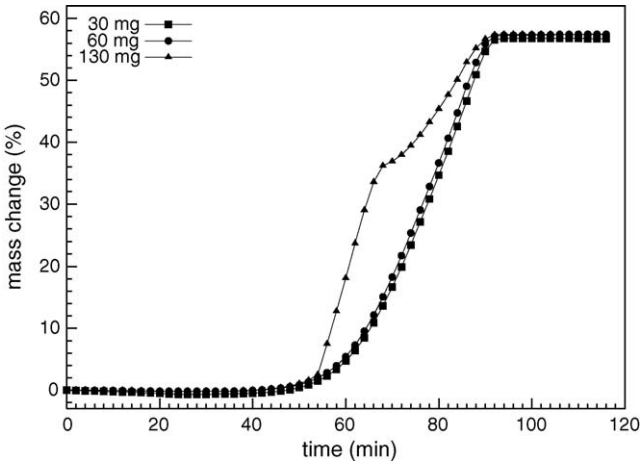


Fig. 5. External heat and mass transfer limitations: oxidation of $ZrAl_3$ powder at a heating rate of 10 °C/min.

The XRD results show that $ZrAl_3$ is oxidized "completely" to $ZrO_2$ and $Al_2O_3$ and that there is no selective oxidation of zirconium which is in accordance with earlier investigations [7].

### 3.2. Effects of mass and heat transfer

To eliminate mass and heat transfer limitations, a series of non-isothermal TG measurements with varying sample masses ranging from 30 to 130 mg were undertaken prior to kinetic analysis. Samples with masses of about 60 mg have powder bed heights less than about 1 mm. The results are presented in Fig. 5 at a heating rate of 10 °C/min. The samples with masses of 30 and 60 mg show similar reaction behaviours indicating that there are no mass transfer limitations through the porous powder bed present. The 130 mg sample size curve differs dramatically. At about 55 min (corresponds to ∼550 °C) the reaction rate increases sharply, then decreases again. In this case the rate of heat generation due to the oxidation reaction exceeds the rate of heat loss and the sample ignites. The temperature rise leads to an increased reaction rate. Finally the reaction rate slows down because of diffusional limitations of the gaseous oxygen and the reaction proceeds kinetically controlled.

Therefore a sample mass of about 60 mg was selected for kinetic analysis. Such a small sample size minimizes the effect of oxygen transportation through the powder volume and self-heating of the sample, while maintaining good relative weighing accuracy. The full data sets which serve as input to the kinetics software are presented in Fig. 6. To verify the reproducibility of the thermogravimetric experiments several non-isothermal runs were repeated and no deviations within the experimental margin of error could be detected.

### 3.3. Kinetic study

In thermal analysis the kinetic evaluation of solid-state or heterogeneous processes is usually based on a single step kinetic

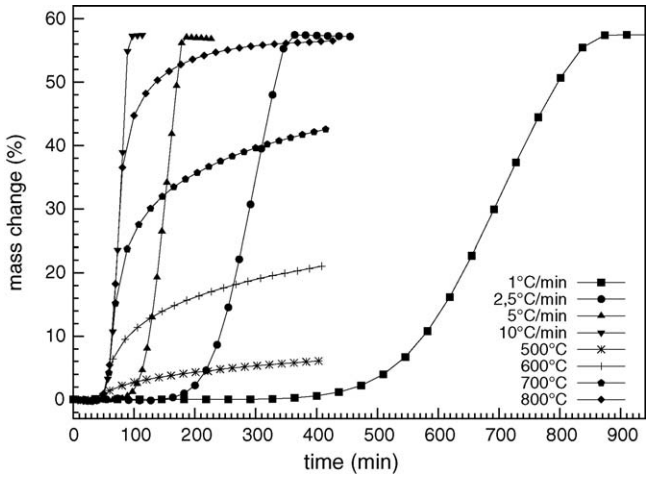


Fig. 6. Isothermal and non-isothermal TG curves for the oxidation of $ZrAl_3$ powder.

equation:

$$\frac{d\alpha}{dt} = k(T)f(\alpha) = A\ \exp\left(-\frac{E_a}{RT}\right) f(\alpha) \quad (2)$$

where $\alpha$ is the conversion degree, in thermogravimetric studies defined as in Eq. (1), $t$ the time, $T$ the temperature, $k(T)$ the rate constant, $A$ the pre-exponential factor, $E_a$ the apparent activation energy and $R$ is the gas constant. For non-isothermal data obtained at a constant heating rate $\beta = dT/dt$, $d\alpha/dt$ in Eq. (2) is replaced with $\beta\, d\alpha/dT$. The above equation may be extended to describe complex processes such as concurrent or consecutive reactions, each with its own kinetic triplet.

To obtain an initial estimate of the kinetic parameters, the method of Friedman was used [11]. Friedman's method is based on taking the natural logarithm of Eq. (2) giving:

$$\ln\left(\frac{d\alpha}{dt}\right)_{\alpha_i} = \ln[Af(\alpha)]_{\alpha_i} - \frac{E_{\alpha_i}}{RT_{\alpha_i}} \quad (3)$$

A plot of $\ln(d\alpha/dt)$ versus $1/T$ at each $\alpha$ yields $E_a$ for that $\alpha$ regardless of the model. Assuming first order kinetics: $f(\alpha) = 1 - \alpha$, an estimate of $A$ can be obtained after transformation of Eq. (3):

$$\ln(A)_{\alpha_i} = \ln\left(\frac{d\alpha}{dt}\right)_{\alpha_i} + \frac{E_{\alpha_i}}{RT_{\alpha_i}} + \ln(1-\alpha_i) \quad (4)$$

If a functional dependence of the activation energy on the extent of conversion results from Friedman analysis, this indicates complexity of the investigated reaction.

The activation energy as a function of conversion of $ZrAl_3$ powder is shown in Fig. 7. As can be seen, the activation energy increases at conversion degrees greater than 0.65. The variable apparent activation energy from the Friedman analysis of the non-isothermal data and the shape of the DTG/DSC curves indicate a change in the reaction mechanism at higher conversion degrees.

To check whether simple one-step models can accurately describe the oxidation kinetics, different reaction models $f(\alpha)$, summarized in Table 1, were evaluated with a non-linear multivariate regression analysis [12]. Table 2 lists the kinetic parameters of the best fitted $f(\alpha)$ models. Neither the phase boundary controlled (R3, R2) nor the diffusion based (D2, D3, D4) and $n$-th order (Fn) mechanisms are able to predict the correct conversion profiles. The inapplicability of these reaction models is demonstrated in Figs. 8(a) and (b), which display the respective best fit for the diffusion models (D4) and reaction-order models (Fn). The experimental data can be well described with a $n$-dimensional Avrami equation (Fig. 8(c)) which is a formal kinetic law and generally applies for random nucleation and growth of nuclei. However at higher conversion degrees, one can observe small deviations from the calculated and experimental data. The calculated apparent activation energy is 244 kJ/mol with a pre-exponential factor $\log(A/s^{-1}) = 9.45$. The small value of the Avrami exponent $n = 0.34$ is relatively close to 0.5, i.e. a value usually taken to indicate a diffusion limited reaction [13]. The $A_{0.5}$ model corresponds to a nuclei growth model, where all nuclei are initially present and the growth process is one-dimensional with diffusion-control [14]. This is in accordance with the fact that the $ZrAl_3$ particles are initially covered with a thin oxide film. During oxidation the growth process continues inwards towards the center of the particles. This type of model for solid-state reactions was also applied to describe the oxidation of Ru powders [15] or the thermal decomposition of aluminium hydride powders [16].

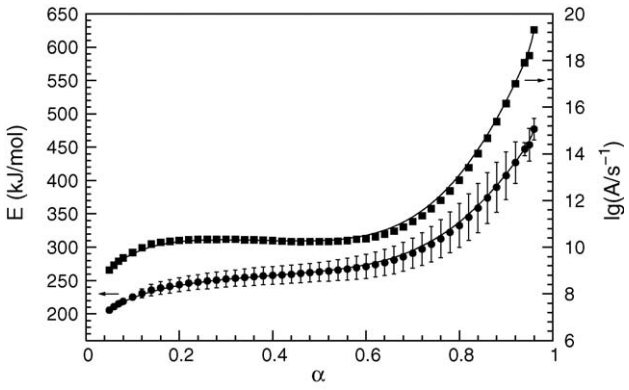


Fig. 7. Friedman analysis of ball milled $ZrAl_3$ powder ($\beta = 1, 2.5, 5$ and 10 °C/min).

As can be seen from Fig. 8(c) there are still some deviations from the calculated and experimental data at higher conversion degrees. The shoulder of the broad exothermic DSC peak and the corresponding peak in the DTG curve at about 900 °C (Fig. 3)

Table 1
$f(\alpha)$ functions for the most common mechanisms in heterogeneous kinetics

| Model | Symbol | $f(\alpha)$ |
|---|---|---|
| One-dimensional diffusion | D1 | $1/2\alpha$ |
| Two-dimensional diffusion | D2 | $-(1/\ln(1-\alpha))$ |
| Three-dimensional diffusion (Jander) | D3 | $3(1-\alpha)^{2/3}/2[1-(1-\alpha)^{1/3}]$ |
| Three-dimensional diffusion (Ginstling–Brounshtein) | D4 | $3/2[(1-\alpha)^{-1/3}-1]$ |
| $n$-th order | Fn | $(1-\alpha)^n$ |
| Phase boundary controlled | Rn ($1 \le n \le 3$) | $n(1-\alpha)^{1-1/n}$ |
| Nucleation and growth (Avrami–Erofeev) | An ($0.5 \le n \le 4$) | $n(1-\alpha)[-\ln(1-\alpha)]^{1-1/n}$ |

indicate an increase of the reaction rate. Therefore a second step was included in the reaction model. The oxidation reaction can best be modelled by two consecutive reactions $A \rightarrow B \rightarrow C$ of the generalized Avrami type An with small exponents $n$ ($n < 1$).

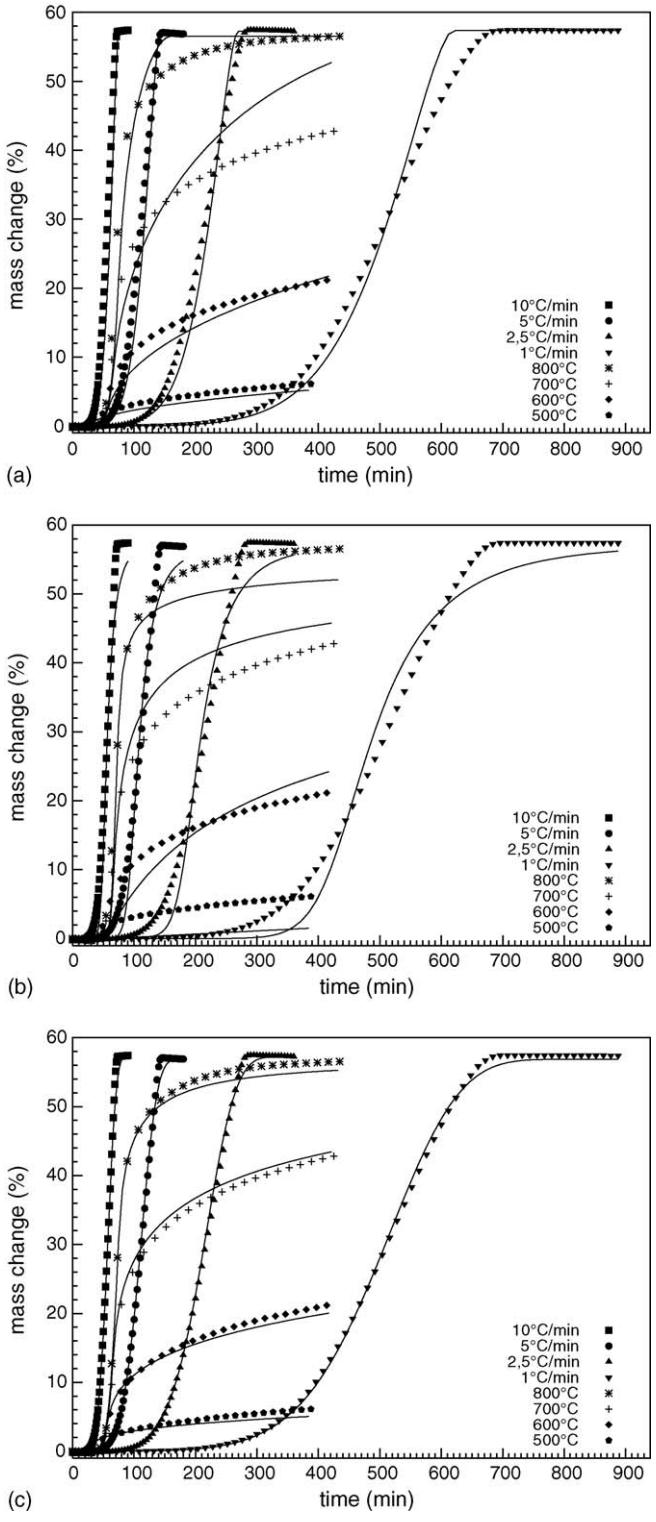


Fig. 8. Comparison of measured and calculated data for non-isothermal and isothermal oxidation of $ZrAl_3$ powder. (a) Best fit model of D4 type, (b) best fit model of Fn type and (c) best fit model of An type (symbols measured, (—) calculated).

The consistency of the kinetic data with this type of rate equation suggests that the oxidation is controlled by a diffusion-limited growth process with a change in diffusive resistance during the reaction. The introduction of the second step leads to more fitting parameters and the model is described by two ordinary differential equations:

$$\frac{da}{dt} = -n_1 \cdot a(-\ln(a))^{1-1/n_1} A_1 \exp\left(-\frac{E_1}{RT}\right),$$

$$\frac{db}{dt} = -\frac{da}{dt} - n_2 \cdot b(-\ln(b))^{1-1/n2} A_2 \exp\left(-\frac{E_2}{RT}\right),$$

$$c = 1 - a - b \quad (5)$$

where $a$, $b$ and $c$ are the relative concentrations of the educt, intermediate reaction product and final product, respectively. The results are shown in Fig. 9, for kinetic parameters see Table 2.

This two-step model is a formal kinetic model and the intermediate reaction product $b$ should be regarded as a pseudo component. A possible interpretation for this two-step behaviour is a change of the physical properties of the growing oxide film because of the formation of two different oxides, the possible existence of partially oxidized amorphous type intermediates and phase transformations in the course of the reaction. Another possible effect is the cracking of the protective oxide film which separates the intermetallic phase and the gaseous oxidant due to mechanical stresses developed during oxidation. A fracture of the oxide film results in an increased reactivity of the intermetallic particles. The apparent kinetic parameters for the initial oxidation ($0.01 \leq \alpha \leq 0.64$) are $E = 226$ kJ/mol, $\log(A/s^{-1}) = 9.26$ and $n = 0.38$. For the latter stage of oxidation ($0.64 < \alpha \leq 0.99$) the calculated kinetic parameters are $E = 280$ kJ/mol, $\log(A/s^{-1}) = 10.27$ and $n = 0.77$. The determined apparent activation energy for the first step is in good agreement with the value of 214 kJ/mol calculated by Paljević [7]. In that study the oxidation of $ZrAl_3$ bars was investigated isothermally in dry oxygen in the temperature range 600–800 °C. The first period of reaction could be described with a logarithmic rate law, but after this initial period the protective oxide film transformed to a porous one and the reaction rate increased. However, it should be mentioned, that the proposed two-step reaction model provides a mathematical expression, which describes the experimental data in the investigated temperature range. The kinetic meaning, especially of the introduced second step, cannot be established. Therefore the model is only valid for the investigated experimental conditions, e.g. temperature range, gas atmosphere and particle size.

According to the X-ray, TG/DSC and kinetic results following simplified oxidation scheme for $ZrAl_3$ powder is proposed:

$$ZrAl_3 \xrightarrow[T>500\,^\circ C]{O_2} 3/2Al_2O_3\,(\text{amorphous})$$

$$+ ZrO_{2-x} \xrightarrow[T>800\,^\circ C]{O_2} 3/2(\gamma, \delta, \theta)\text{-}Al_2O_3 + \text{t-}ZrO_2 \quad (6)$$

Finally, at temperatures of about 1100 °C, the transition aluminas transform into the thermodynamically stable $\alpha$-$Al_2O_3$ modification.

Table 2
Comparison of selected results of multiple-curve analysis of the thermal oxidation of $ZrAl_3$ powder with one- and two-step reaction patterns

| | Reaction type(s) | Parameter | Value | Correlation-coefficient | $F_{exp}$ | $F_{crit(0,95)}$ |
|---|---|---|---|---|---|---|
| d:f | An | $\log(A_1/s^{-1})$ | 9.26 ± 0.075 | 0.99973 | 1.00 | 1.07 |
| | | $E_1$/kJ mol$^{-1}$ | 226 ± 2 | | | |
| | | $n_1$ | 0.384 ± 0.003 | | | |
| | An | $\log(A_2/s^{-1})$ | 10.27 ± 0.11 | | | |
| | | $E_2$/kJ mol$^{-1}$ | 280 ± 3 | | | |
| | | $n_2$ | 0.765 ± 0.02 | | | |
| | | FollReact.1[a] | 0.64 ± 0.02 | | | |
| s | An | $\log(A/s^{-1})$ | 9.45 ± 0.009 | 0.99908 | 3.37 | 1.07 |
| | | $E$ /kJ mol$^{-1}$ | 244 ± 2 | | | |
| | | $n$ | 0.337 ± 0.003 | | | |
| s | D3 | $\log(A/s^{-1})$ | 4.32 ± 0.10 | 0.99064 | 34.41 | 1.07 |
| | | $E$/kJ mol$^{-1}$ | 169 ± 2 | | | |
| s | Fn | $\log(A/s^{-1})$ | 7.91 ± 0.26 | 0.98700 | 47.46 | 1.07 |
| | | $E$/kJ mol$^{-1}$ | 199 ± 4 | | | |
| | | $n$ | 3.51 ± 0.10 | | | |
| s | D4 | $\log(A/s^{-1})$ | 3.79 ± 0.11 | 0.98618 | 50.66 | 1.07 |
| | | $E$/kJ mol$^{-1}$ | 161 ± 2 | | | |
| s | D2 | $\log(A/s^{-1})$ | 4.21 ± 0.009 | 0.98309 | 61.92 | 1.07 |
| | | $E$/kJ mol$^{-1}$ | 158 ± 2 | | | |
| s | R2 | $\log(A/s^{-1})$ | 3.34 ± 0.12 | 0.96885 | 113.10 | 1.07 |
| | | $E$/kJ mol$^{-1}$ | 134 ± 2 | | | |
| s | R3 | $\log(A/s^{-1})$ | 2.68 ± 0.16 | 0.94567 | 194.38 | 1.07 |
| | | $E$/kJ mol$^{-1}$ | 127 ± 3 | | | |

s, Single step; d:f, two consecutive steps.

[a] Share of step 1 in the total mass increase.

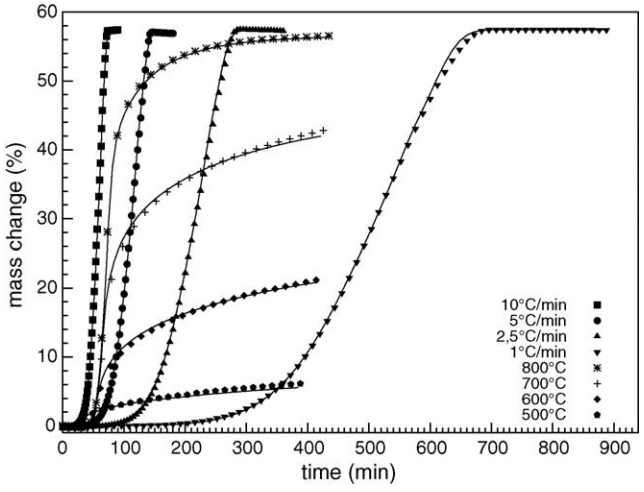


Fig. 9. Comparison of measured and calculated data for non-isothermal and isothermal oxidation of $ZrAl_3$ powder. Two-step model of type $A \rightarrow^1 B \rightarrow^2 C$ with 1: An, 2: An (symbols measured, (—) calculated).

## 4. Conclusions

Non-isothermal and isothermal oxidation of ball milled $ZrAl_3$ powder was investigated up to temperatures of 1100 °C under flowing air using thermogravimetry. The non-selective oxidation of $ZrAl_3$ results in the formation of $\alpha$-$Al_2O_3$, tetragonal and monoclinic $ZrO_2$. The oxidation kinetics can be described with a generalized *n*-dimensional Avrami type equation indicating a diffusion controlled oxidation mechanism. The deviation of the kinetic exponent from the ideal value of 0.5 is most likely due to the non-ideal monodisperse powder. A considerable improvement of the fit quality of the TG data is achieved by a two-step kinetic model. A sound explanation of the multi-step nature of the oxidation process solely based on TG measurement is difficult and therefore additional measurement techniques are necessary. A possible explanation is the change of the physical properties of the protecting oxide film or the formation of cracks.

The determined kinetic model can be incorporated in a more detailed reaction-diffusion model taking into account the diffusion of oxygen through a porous $ZrAl_3$ green body and an energy balance. The reaction-diffusion model can be used to describe the oxidation bevaviour of $ZrAl_3$ green bodies during the reaction bonding of alumina-zirconia composites. With the help of this model the influence of several processing parameters like sample size or heating cycle on the reaction behaviour can be investigated. This is the subject of a following paper.

## References

[1] N. Claussen, T. Le, S. Wu, Low-shrinkage reaction-bonded alumina, J. Eur. Ceram. Soc. 5 (1989) 29–35.
[2] G. Ziegler, J. Heinrich, G. Wotting, Relationships between processing, microstructure and properties of dense reaction-bonded silicon nitride, J. Mater. Sci. 22 (9) (1987) 3041–3086.
[3] V. Hlavacek, J.A. Puszynski, Chemical Engineering Aspects of Advanced Ceramic Materials, Industr. Eng. Chem. Res. 35 (1996) 349–377.
[4] V.D. Hennige, J. Haußelt, H.-J. Ritzhaupt-Kleissl, T. Windmann, Shrinkage-free $ZrSiO_4$-ceramics: characterisation and applications, J. Eur. Ceram. Soc. 19 (1999) 2901–2908.

[5] H. Geßwein, J.R. Binder, H.-J. Ritzhaupt-Kleissl, J. Haußelt, Fabrication of net shape reaction bonded oxide ceramics, J. Eur. Ceram. Soc. 26 (2006) 697–702.
[6] M. Paljević, Change of oxidation kinetics in the Zr-Al-System, J. Less-Comm. Met. 157 (1990) 289–293.
[7] M. Paljević, Non-selective oxidation of $ZrAl_3$, J. Less-Comm. Met. 175 (1991) 289–294.
[8] M. Paljević, High-temperature oxidation behaviour in the Zr-Al system, J. Alloys Compd. 204 (1994) 119–126.
[9] J. Opfermann, Netzsch Thermokinetics 2, Version 2004.05, Netzsch Gerätebau GmbH.
[10] B.C. Lippens, J.H. de Boer, Study of phase transformations during calcination of aluminum hydroxides by selected area electron diffraction, Acta Crystallogr. 17 (1964) 1312–1321.
[11] H.L. Friedman, Kinetics of thermal degradation of char-forming plastics from thermogravimetry—application to a phenolic plastic, J. Polym. Sci. Part C 6 (1965) 183–195.
[12] J. Opfermann, Kinetic analysis using multivariate non-linear regression, J. Therm. Anal. Calorimetry 60 (2000) 641–658.
[13] C.H. Bamford, C.F.H. Tipper (Eds.), Reactions in the solid state, in: Comprehensive Chemical Kinetics, vol. 22, Elsevier, 1980 (Chapter 3).
[14] S.F. Hulbert, Models for solid-state reactions in powdered compacts—a review, J. Br. Ceram. Soc. 6 (1969) 11–20.
[15] M. Prudenziati, B. Morten, E. Travan, Reduction process of $RuO_2$ powders and their re-oxidation, Mater. Sci. Eng. B98 (2003) 167–176.
[16] I.M.K. Ismail, T. Hawkins, Kinetics of thermal decomposition of aluminium hydride. I. Non-isothermal decomposition under vacuum and inert atmosphere (argon), Thermochim. Acta 439 (2005) 32–43.